Journal of Materials Chemistry A

Accepted Manuscript

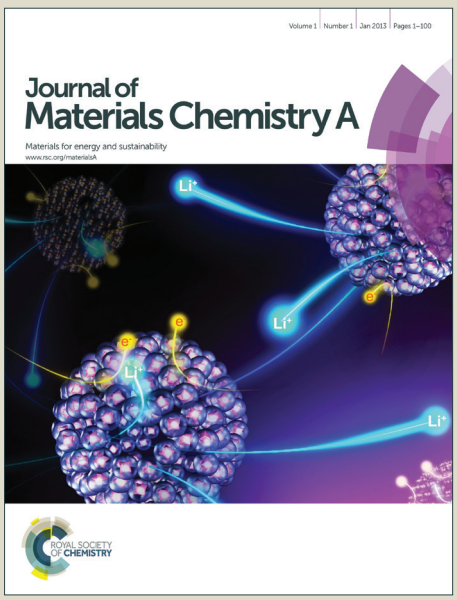

ROYAL SOCIETY OF CHEMISTRY

www.rsc.org/materialsA

A **Table of Contents Entry for *J. Mater. Chem. A***

Yujing Luo, Xiaoming Liu*, Xinghua Tang, Yan Luo, Qianyao Zeng, Xiaolei Deng, Shaolei Ding, Yiqun Sun

J. Mater. Chem. A, **2014**, *xx*, xxxx

Gold Nanoparticles Embedded in Ta_2O_5 /Ta_3N_5 as Active Visible-light Plasmonic Photocatalysts for Solar Hydrogen Evolution

The Nano Au/Ta_2O_5 composite shows a new recreating photocatalytic activity for hydrogen evolution from water response to visible light irradiation.

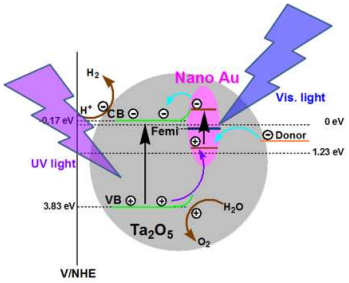

Gold Nanoparticles Embedded in Ta_2O_5 /Ta_3N_5 as Active Visible-light Plasmonic Photocatalysts for Solar Hydrogen Evolution

Yujing Luo,[†] Xiaoming Liu,*[,†] Xinghua Tang,[†] Yan Luo,[†,‡] Qianyao Zeng,[†] Xiaolei Deng,[†] Shaolei Ding,[†] Yiqun Sun[†]

[†]School of Environment and Chemical Engineering, Nanchang Hangkong University, Nanchang 330063, P. R. China.
[‡]Key Laboratory of Jiangxi Province for Persistant Pollutants Control and Resources Recycle, Nanchang Hangkong University, Nanchang 330063, P. R. China.

Abstract

Here, we demonstrate a new recreating photocatalytic activity of Nano Au/Ta_2O_5 composite for hydrogen evolution from water as a visible-light responsive plasmonic photocatalyst by embedding Au nanoparticles in Ta_2O_5 host lattice. The Nano Au/Ta_2O_5 composite samples were prepared through a simple Pechini-type sol-gel process. Further nitridating Nano Au/Ta_2O_5 composite samples in ammonia flow at 1123 K to get Nano Au/Ta_3N_5 composite samples. The obtained Nano Au/Ta_3N_5 composite exhibited a significantly enhanced photocatalytic activity in visible region for hydrogen evolution from water comparing with blank Ta_3N_5 nanoparticles. UV-Vis diffuse reflectance spectra and photocatalytic activity measurements indicated that the excitation of surface plasmon resonance of Au nanoparticles is responsible for the new recreating photocatalytic activity of Nano Au/Ta_2O_5 composite and significantly enhanced photocatalytic activity in Nano Au/Ta_3N_5 composite for hydrogen evolution in visible region, which might be ascribed to the charge transfer effect in Nano Au/Ta_2O_5 composite and the synergetic effect of charge transfer and near-field electromagnetic effect in Nano Au/Ta_3N_5 composite induced by surface plasmon resonance of embedded Au nanoparticles. The current study could provide a new paradigm for designing plasmonic metal/semiconductor composite systems for photocatalysts, photovoltaics and other optoelectronic devices.

Keywords: Nano Au/Ta_2O_5 (Ta_3N_5) composite, plasmonic photocatalyst, hydrogen evolution.

---

* To whom correspondence should be addressed. E-mail: xmliu2014@163.com

1 Introduction

Due to global environmental problems and energy issues, scientists have paid a great deal of attention to the utilization of solar energy for the production of hydrogen from water using photocatalysts.[1-4] Although several metal oxide semiconductors have been reported to be active photocatalysts for the overall water splitting reaction, most only function under ultraviolet (UV) light ($\lambda < 400$ nm) because of their large band gap (> 3 eV)[5-12] With respect to the solar spectrum, only a small fraction (ca. 4%) of the incoming solar energy lies in the ultraviolet region, whereas the visible light in solar spectrum is far more abundant (ca. 46%). It is extremely important, therefore, to develop visible-light-driven photocatalysts that are stable and highly efficient for the practical, large-scale production of hydrogen using solar energy.[13-16]

The recent and rapid development of surface plasmon resonance (SPR) has offered a new opportunity to overcome the limited efficiency of photocatalysts and photovoltaic devices. The visible-light-triggered plasmonic photocatalysts have been recognized as one of the most promising alternatives to the traditional photocatalysts.[17-19] Incorporating plasmonic metal nanostructures into semiconductors can increase the efficiency of photovoltaic devices by 10 ~15 % and enhances photocatalytic activity toward organic compound decomposition and water splitting.[20-27]

Currently, three primary enhancement mechanisms, often termed as charge transfer mechanism, near-field electromagnetic effect mechanism and photon scattering effect mechanism, have been proposed by which metal SPR improves the solar-energy-conversion efficiency on nearby semiconductors.[17,18] Tian et al. reported that visible-light irradiation ($\lambda >$ 420 nm) of Au nanoparticles on a semiconductor film coated on an indium tin oxide electrode generates an anodic photocurrent in the presence of Fe^{2+}.[28] This photoelectrochemical response

is explained by an electron transfer mechanism similar to that for dye-sensitized TiO_2. Collective oscillation of electrons on Au nanoparticles induced by the incident light transfer conduction electrons (e^-) from Au nanoparticles to TiO_2 conduction band, and the positively charged Au nanoparticles received e^- from electron donor (Fe^{2+}). Similar phenomena have been discovered in other plasmon-induced photocatalysts, such as, in Ag-AgI/Al_2O_3, Pt/P25, Au/P25, Au/TiO_2.[25,29-32] Beside direct electron transfer occurs from plasmonic metal to the conduction band of semiconductor, plasmonic resonant energy transfer mechanism has also been proposed by Wu et al. in Au@SiO_2@Cu_2O.[17] Comparing with direct electron transfer, resonant energy transfer from a plasmonic metal to a semiconductor overcome the limitation of the required electronic band alignment, offering much more flexibility for designing photocatalysts, photovoltaics, and other optoelectronic devices.[17]

It was reported that the interaction of localized electric fields with a neighboring semiconductor can allow for the facile formation of electron-hole (e^--h^+) pairs in the near-surface region of the semiconductor.[27] Furthermore, the SPR-induced electric field in the interface of metal nanostructures and semiconductors can effectively separate the photogenerated charge carriers.[33] These factors in turn will result in higher photocatalytic activity of plasmonic photocatalyst. Cronin et al. observed enhancements of up to 66 times in the photocatalytic water splitting in Nano Au/TiO_2 composites under visible illumination comparing to TiO_2 alone.[27] Electromagnetic simulations indicate that the improvement of photocatalytic activity in visible range is caused by the local electric field enhancement near TiO_2 surface. Li et al. studied the Au/TiO_2/Au nanostructure as a plasmonic coupling photocatalyst.[33] The three-dimensional finite-difference simulations show that the superior photoelectrochemicl properties of Au/TiO_2/Au was mainly attributed to the localized electric field enhancement on TiO_2 surface coming from the

plasmonic coupling resonance effect of Au nanoparticles.[33] Linic et al. demonstrated the SPR-induced near-field electromagnetic effect in Ag/N-TiO_2 and Au/N-TiO_2 plasmonic-metal/semiconductor composites for their enhanced water splitting performance in response to visible light irradiation.[34] For photon scattering effect mechanism, it is usually based on efficient scattering of resonant photons by plasmonic nanostructures, resulting in longer optical path lengths for photons in semiconductor matrix that yields a higher rate of the formation of excited charge carries.[26,27]

So far, although some noble metal nanoparticle/semiconductor oxide composites have often been investigated as plasmonic photocatalysts, yet most of them are restricted to noble metal nanoparticles/TiO_2 composites, such as Au/TiO_2, Au/TiO_2/Au, Pt/P25, Au/P25, Pt/TiO_2, Au/TiO_2, Ag/N-TiO_2 and Au/N-TiO_2 etc..[25,29-36] Besides TiO_2, there is very limited report of other (noble metal nanoparticles/) semiconductor composites as plasmonic photocatalysts. So it is of great interest and importance to extend research of plasmonic photocatalysts to other (noble metal nanoparticles/) semiconductor composites, such as (noble metal nanoparticles/) Ta_2O_5, Ta_3N_5, TaON, $SrTiO_3$, $La_2Ti_2O_7$, etc..

Tantalum oxide (Ta_2O_5) has found many applications in different research fields, including used as a protective coating material, catalyst, capacitor, resistor, optical device, as well as a biomedical material.[37,38] Especially, Ta_2O_5 has been extensively investigated as a photocatalyst (or photoanode) for photoelectrochemical water splitting because of its favorable band-edge positions, strong optical absorption, superior chemical stability, photocorrosion resistance, and low cost.[39,40] However, the solar-to-hydrogen efficiency of Ta_2O_5 is substantially limited by its large band gap energy (4.0 eV) and usually fast electron hole recombination due to a high density of trap states.[41,42] As a homologous compound of Ta_2O_5, tantalum(V) nitride (Ta_3N_5) has

attracted tremendous attention as a visible-light-responsive photocatalyst.[43,44] It has a band gap energy of 2.08 eV and thus can absorb a large fraction of visible light < 600 nm. Ta_3N_5 has been reported to produce hydrogen or oxygen in the presence of appropriate sacrificial reagents and visible-light irradiation,[45,46] suggesting that the band positions for valence/conduction bands are suitable for overall water splitting. However, the photocatalytic activity efficiency of Ta_3N_5 remains low and must be greatly improved for practical applications in the future.[47,48]

As far as we know, there is no any report about Nano Au/Ta_2O_5 (Ta_3N_5) plasmon nanostructure. Furthermore, key factor that is effective for hydrogen evolution in noble metal nanoparticle/semiconductors plasmonic photocatalysts has not been investigated in detail. Accordingly, in the present study, we reported the synthesis of Nano Au/Ta_2O_5 and Nano Au/Ta_3N_5 composite plasmon photocatalysts with embedded and surface configurations, and investigated the crystallinities, morphologies, structures, optical properties, photocatalytic performances and photocatalytic mechanism of the prepared samples in more detail. The Nano Au/Ta_2O_5 composite plasmon photocatalyst was prepared by a simple Pechini-type sol-gel process. For Nano Au/Ta_3N_5 composite plasmon photocatalyst, it was prepared by a nitriding process under ammonia atmosphere at high temperature using the obtained Nano Au/Ta_2O_5 composite as precursor. It is of interest and significance to find that the Nano Au/Ta_2O_5 composite shows a new recreating photocatalytic activity for hydrogen evolution from water with comparable efficiency under the irradiation of visible light comparing to blank Ta_2O_5, and the Nano Au/Ta_3N_5 composite shows a significantly enhanced photocatalytic activity for hydrogen evolution from water response to visible light illumination comparing to Ta_3N_5 alone. Considering the versatility and flexibility of plasmon metal nanoparticle/semiconductor

composite, this work may provide some insights into the design of novel and highly efficient photocatalysts, photovoltaics and other optoelectronic devices.

2 Experimental

2.1 Synthesis of Au nanoparticles

Citric acid (99.99%) and trisodium-citrate were supplied by Sigma. Tetrachloroauric acid trihydrate (99.99%) were supplied by Sigma-Aldrich. All chemicals were used without further purification and Mili-Q water was used throughout. Au nanoparticles were prepared by the standard citrate reduction method with some modification.[49] Briefly, 4.0 ml of $H[AuCl_4].3H_2O$ solution (2% w/v) in 50 mL of water were heated to boiling and then 4.0 ml of trisodium-citrate solution (10% w/v, 0.5 % w/v citric acid) were added quickly under vigorous stirring. The solution was kept boiling for 2 min, then it was allowed to cool down to room temperature to obtain the stock solution of Au nanoparticles.

2.2 Synthesis of Au nanoparticles embedded in Ta_2O_5 and Ta_3N_5 bulk samples

The blank Ta_2O_5 and Nano Au/Ta_2O_5 composite (Au nanoparticles embedded in Ta_2O_5) samples all were prepared by a Pechini-type sol–gel process.[48] The embedding concentrations of Au nanoparticles are 0.36–1.44 mol% of Ta_2O_5. Tantalum pentachloride (99.99% $TaCl_5$, Sigma-Aldrich) was used as a starting material to prepare the Au nanoparticles embedded in Ta_2O_5 samples. An appropriate amount of $TaCl_5$ was dissolved in absolute alcohol to obtain a clear $TaCl_5$ solution, and a suitable amount of water-ethanol (v/v=1:7) solution containing citric acid (≥ 99.5%, Sigma-Aldrich) was added into $TaCl_5$ solution as a chelating agent for the metal ions. The molar ratio of metal ions to citric acid was 1:2. As a cross-linking agent, a suitable amount

of polyethylene glycol (PEG, molecular weight = 10 000, Bio Ultra, Sigma) was added with a final concentration of 0.20 $g \cdot ml^{-1}$, and the pH value of the solution was maintained between 4 and 6. A highly transparent sol was obtained after stirring for 2 h. After that, the stock solution of Au nanoparticles was added into the above transparent sol under stirring. After adding the stock solution of Au nanoparticles, the transparent sol changes into deep red color accordingly. The red color does not fade out even it is kept for a few days, indicating that there is no aggregation or precipitation of Au nanoparticles in the deep red sol, which might be due to the Au nanoparticles are stabilized by citrate and PEG. The deep red sol was stirred for 3h and heated at 80 ^{o}C in a water bath until homogenous deep gels formed. After being dried in an oven at 110 ^{o}C for 10 h, the gels were ground and prefired at 450 ^{o}C for 4h in air. Then the samples were fully ground and calcinated at desired temperatures for 3h in air to produce the final samples of Nano Au/Ta_2O_5 composite. To prepare Nano Au/Ta_3N_5 composite, the obtained Nano Au/Ta_2O_5 composite precursor was placed in a tube furnace and subjected to nitridation in a flow of ammonia gas with a flow rate of 150 ml/min at 750 ^{o}C for 8h. The sample was taken out from the furnace after cooling to room temperature in a flow of N_2 gas. For comparison, the blank samples of Ta_2O_5 and Ta_3N_5 were also prepared by same processes as those of Au/Ta_2O_5 and Au/Ta_3N_5 composite without Au nanoparticle embedding, respectively.

2.3 Photocatalytic reactions

Photocatalytic reactions were performed in a Pyrex top-irradiation reaction vessel connected to a glass closed-gas circulation system. The reactant solutions were evacuated several times to completely remove any air prior to irradiation with a 300 W xenon lamp. The irradiation wavelength was controlled with a combination of a cold mirror (CM-1 for visible light, CM-2 for UV light) and a water filter ($200 < \lambda < 800$ nm). For visible light irradiation, a long pass filter

(L42) was fitted to the aforementioned light source ($420 < \lambda < 800$ nm). The reactant solution was maintained at room temperature using a flow of cooling water during the reaction. For H_2 evolution, the reactions were performed using an aqueous solution (100 mL) with 0.06 g of catalyst suspended by magnetic stirring and MeOH (10 vol %) as a sacrificial electron donor. The Pt (0.5 ~ 3 wt %) co-catalyst was loaded onto the photocatalysts via impregnation, followed by H_2 reduction at 300 ^{o}C for 2 h. For O_2 evolution, 0.01M $AgNO_3$ is used as a sacrificial electron acceptor and 0.05g La_2O_3 are used to keep the pH value of solution stabile. Except for sacrificial reagent, the other experimental procedures are similar to those of H_2 evolution. Evolved gases were analyzed using gas chromatography (Ar carrier, thermal conductivity detector, and MS-5A column) connected directly to the closed-gas circulation system.

2.4 Characterization

X-ray diffraction (XRD) patterns of the products were collected on a Bruker DMAX 2500 X-ray diffractometer using Cu Kα radiation (k = 0.154 nm). Environmental in situ SEM was conducted on an FEI Quanta 600 microscope with a gaseous secondary electron detector operated at 5 KV. Bright-field TEM and high-angle annular dark-field STEM images were acquired on an FEI Titan ST electron microscope (C_s=1.2 mm; C_c=1.5 mm; 300 kV). Diffuse reflectance spectra were obtained using a JASCO V-560 UV-visible diffuse reflectance spectrometer equipped with an integration sphere using Spectralon as a reference and were converted from reflection to absorbance by the Kubelka-Munk method. All the measurements were performed at room temperature.

3 Results and discussion

3.1 Crystallization behavior and morphology

Figure 1 shows the representative X-ray diffraction patterns for blank Ta_2O_5 nanocrystllines (NCs) annealed at 750 ^oC (a), Nano Au/Ta_2O_5 composite (Au nanparticles embedded in Ta_2O_5) annealed at 750 ^oC (b, Nano Au 1.44 mol% of Ta_2O_5), blank Ta_3N_5 NCs nitrided at 750 ^oC (c) and Nano Au/Ta_3N_5 composite (Au nanparticles embedded in Ta_3N_5) nitrided at 750 ^oC (d, Nano Au 2.17 mol% of Ta_3N_5). For blank Ta_2O_5 NCs (a) and Nano Au/Ta_2O_5 composite (b), the diffraction peaks can be basically indexed to the standard data of Ta_2O_5 (JCPDS 25-0922). For Nano Au/Ta_2O_5 composite, no second phase was detected at the current Au nanparticles embedding level, indicating that there is no any chemical reaction for Au nanparticles and Ta_2O_5 NCs. After the blank Ta_2O_5 NCs and Nano Au/Ta_2O_5 composite were nitrided under the ammonia flow at 750 ^oC for 8 h, XRD patterns matching those of the Ta_3N_5 crystal structure (JCPDS 19-1291) were observed (Figure 1c for Ta_3N_5 and Figure 1d for Nano Au/Ta_3N_5 composite). No diffraction peaks of Au nanoparticle species were observed in Nano Au/Ta_2O_5 composite (b) and Nano Au/ Ta_3N_5 composite (d). This presumably was ascribed to the incorporation of Au nanoparticles with low content, small particle size, and homogeneous dispersion in Ta_2O_5 and Ta_3N_5 matrixes.

One of the virtues of Pechini-type sol–gel process is the homogeneously mixing the staring materials at molecular level. In sol–gel process, citric acid first chelates Ta^{5+}, and the remaining carboxylic acid groups in citric acid react with polyethylene glycol to form polyester with suitable viscosity.[48,50] When Au nanoparticle stabilized by citric acid in water was added into the sol, the same thing happened to Au nanoparticle, the carboxylic acid groups on the surface of Au nanoparticle will also react with polyethylene glycol to form polyester, which accordingly make Au nanoparticles to disperse in sol homogeneously.

To illustrate how crystallinity of Nano Au/Ta_2O_5 composite changes with annealing

temperature, the XRD of Nano Au/Ta_2O_5 composite samples (Nano Au 1.08 mol% of Ta_2O_5) annealed at different temperatures are shown in supporting information 1 (SP1). The blank Ta_2O_5 sample annealed at 750 ^oC is also shown in SP1 for comparison. For the sample annealed at 550 ^oC, only some amorphous phases are present, and no diffraction peaks of the desired Ta_2O_5 can be seen. The diffraction peaks of Ta_2O_5 appeared only when the sample was annealed at 600 ^oC, indicating that the Ta_2O_5 began to crystallize at this temperature. Single-phase Ta_2O_5 with an orthorhombic structure was obtained after annealing at 650 ^oC. Obviously, the intensity of XRD signals and the crystallinity of the prepared samples increased with annealing temperature.[51,52] All diffraction peaks of the Nano Au/Ta_2O_5 sample annealed at 650 ℃ or higher temperature can be assigned exactly to the standard data of Ta_2O_5 (JCPDS 25-0922).[53] Usually, the higher annealing temperature can significantly improve the lattice integrity and crystallinity of the Nano Au/Ta_2O_5 nanoarchitectures, which will optimize their photocatalytic activities for H_2 evolution accordingly.[50]

The crystallite size of the samples can be estimated from the Scherrer equation, $D = 0.941\lambda/\beta\cos\theta$, where D is the average grain size, λ is the X-ray wavelength (0.15405 nm), θ and β are the diffraction angle and full-width at half-maximum of an observed peak, respectively.[50] The strongest peak ($2\theta = 22.9°$) was used to calculate the average crystalline size (D) of the Nano Au (1.44 mol%) /Ta_2O_5 composite. The estimated average crystallite size of Nano Au/Ta_2O_5 sample is about 38 nm. For comparison, the average crystalline size (D) of blank Ta_2O_5 sample is estimated to be 32 nm. It shows that the embedding Au nanoparticles have induced larger crystalline size of Ta_2O_5 sample to some extent.

Figure 2 shows the SEM of blank Ta_2O_5, Nano Au/Ta_2O_5 composite (Au 1.44 mol% of Ta_2O_5), blank Ta_3N_5 and Nano Au/Ta_3N_5 composite (Au 2.17 mol% of Ta_3N_5). From Figure 2a,

it can be observed that the blank Ta_2O_5 sample is composed of aggregated particles with size ranging from 150 to 200 nm. This reflects the polycrystalline nature of the blank Ta_2O_5 sample, i.e., each particle contains a lot of individual crystallites. For Nano Au/Ta_2O_5 composite (shown in Figure 2b), it does not show much difference from blank Ta_2O_5 in morphologies and particles size range. A detailed examination of SEM micrograph indeed indicates that each particle of the prepared sample consists of many smaller crystallites (20-50 nm for blank Ta_2O_5 and Nano Au/Ta_2O_5 composite), which basically agrees with those (32.0 nm for blank Ta_2O_5 and 38.0 nm for Nano Au/Ta_2O_5 composite, respectively) estimated from the Scherrer equation. After nitriding Ta_2O_5 and Nano Au/Ta_2O_5 in ammonia flow at high temperature, due to the chemical reaction and phase transformation, the morphologies of the prepared Ta_3N_5 (Figure 2c) and Nano Au/Ta_3N_5 composite (Figure 2d) become a little bit aggregated and show bigger particle sizes comparing to those of the blank Ta_2O_5 and Nano Au/Ta_2O_5 composite samples. Furthermore, it can be seen obviously that the aggregation of Nano Au/Ta_3N_5 composite seem more serious than that of blank Ta_3N_5. The estimated size of blank Ta_3N_5 and Nano Au/Ta_3N_5 composite are estimated to range from 170 to 250 nm, and 200 to 350 nm, respectively. It shows that the embedding Au nanoparticle affects the morphology and size of Nano Au/Ta_3N_5 composite a little bit.

Figure 3 shows the TEM of Au nanoparticle (Figure 3a), high-angle annular dark-field STEM (HAADF-STEM) images of blank Ta_2O_5 (Figure 3b) and Nano Au/Ta_2O_5 composite (Figure 3c), Energy-dispersive X-ray spectroscopy (EDS) of Nano Au/Ta_2O_5 composite (Figure 3d), HAADF-STEM images of blank Ta_3N_5 (Figure 3e) and Nano Au/Ta_3N_5 composite (Figure 3f), EDS of Nano Au/ Ta_3N_5 composite (Figure 3g) and HRTEM of Nano Au/Ta_2O_5 composite loaded with Pt nanoparticle as cocatalyst (Figure 3h). As shown in Figure 3a, the Au

nanoparticles are monodisperse with size around 15 ~ 20 nm. The diffraction fringes in different crystal orientation show high crystallinity of Au nanoparticles. The blank Ta_2O_5 and Ta_3N_5 (Figure 3b for Ta_2O_5 and Figure 3e for Ta_3N_5) shown here for comparison are composed of small particles of 30 ~ 100 nm with some aggregation. The Au nanoparticles were observed as white spots having obvious contrast with the Ta_2O_5 and Ta_3N_5 support as shown in Figure 3c and Figure 3f, respectively. From Figure 3c and 3f, it is clearly seen that the Au nanoparticles are uniformly dispersed in Ta_2O_5 and Ta_3N_5 host lattices. Even after a series of calcination procedures, the size of Au nanoparticles still do not change. This may be due to Au nanoparticles are homogeneous dispersed in Ta_2O_5 (Ta_3N_5) precursors, and they are isolated each other by Ta_2O_5 (Ta_3N_5) host lattice. This isolation prevents them from growing up and keeps them still in original sizes. The EDS of Nano Au/Ta_2O_5 (Figure 3d), Nano Au/Ta_3N_5 (Figure 3g), Nano Au/Ta_2O_5-Pt (Supporting Information 2, SP2), and Nano Au/Ta_3N_5-Pt (SP2) suggest that the existence of Ta (from Ta_2O_5), O (from Ta_2O_5), N (from Ta_3N_5), Cu (from the grid), Au (from embedded Au nanoparticles), and Pt (from Pt nanoparticles loaded as cocatalysts). The high-resolution transmission electron microscopy (HRTEM) images of Nano Au/Ta_2O_5-Pt (Figure 3h) clearly shows that the Au nanoparticles were embedded in Ta_2O_5 and well-defined contact surfaces between the Au nanoparticles and Ta_2O_5. The Pt nanoparticle loaded as cocatalyst on the surface of Ta_2O_5 for photocatalytic reaction also can be seen separately and well contact with Ta_2O_5 host lattice. In Figure 3h, the HRTEM image taken at the interface of Ta_2O_5 and Au nanoparticles regions clearly revealed two distinct sets of lattice fringes, which can be assigned to the Ta_2O_5 and Au nanoparticles, respectively. Note that this sharp interface of Au nanoparticles and Ta_2O_5 in Nano Au/Ta_2O_5 composite is believed to be important for excited electron injection from Au nanoparticles to Ta_2O_5 upon SPR excitation.[18,19]

3.2 Optical properties

The Au nanoparticles can be firmly embedded in Ta_2O_5 and Ta_3N_5 host lattices. It exhibits a characteristic surface plasmon resonance absorption band ranging from ultraviolet (UV) to visible light region due to the collective excitation of electrons, which was induced by the incident electromagnetic radiation in gold nanoparticles.[26,30] Figure 4 show the UV-vis absorption spectra of blank Ta_2O_5, Nano Au/Ta_2O_5 composite (Figure 4a), blank Ta_3N_5 and Nano Au/Ta_3N_5 composite (Figure 4b). The absorption spectrum of the stock solution of Au nanoparticles is also shown in Figure 4 for comparison. For Ta_2O_5 without Au nanoparticle embedding in, it absorbs only UV light. There is a strong absorption band at $\lambda < 310$ nm, then the optical absorption of Ta_2O_5 decreased sharply at wavelengths longer than 310 nm due to the limitation of wide band gap energy (around 4.0 eV). The UV/visible absorption/extinction of the stock solution of Au nanoparticles shows a localized surface plasmon resonance (LSPR) absorption band maximizing at 518 nm with a shoulder around 360 nm. After Au nanoparticles were embedded in Ta_2O_5, the Nano Au/Ta_2O_5 composite shows not only the absorption band of Ta_2O_5 peaking at 263 nm, but also the characterized LSPR absorption of Au nanoparticle in range from 310 to 900 nm peaking at 596 nm with a shoulder at 443 nm. As it is known that the frequency of the LSPR can be reasonably tuned by changing the size, shape, and dielectric environment of the particles.[26,27] The dielectric constant for Ta_2O_5 is around 30.0, while for H_2O, it is 1.0. When Au nanoparticle was embedded in Ta_2O_5, the LSPR absorption band red shifts from ca. 518 nm to ca. 596 nm, which primarily due to the increase in the dielectric constant of the surrounding medium. A monotonic increase in intensity of the absorption band peaking at 596 nm with a shoulder at 443 nm was observed with increasing the embedding Au nanoparticle concentration in Nano Au/Ta_2O_5 composite, until finally the LSPR absorption band peaking at

596 nm has comparable intensity to the band gap transition band of Ta_2O_5 peaking at 263 nm.

The UV-vis absorption spectra of Ta_3N_5 (Figure 4b, black line) shows strong absorption bands in range from 200 to 650 nm, which are due to the electron transition from valence bands (consisting of the 2p orbital of N) to the conduction bands (consisting of the 5d orbital of Ta), and weak background absorption band in range from 650 to 900 nm. The background level absorption corresponds to the presence of reduced species or anion defects.[46,48] For Nano Au/Ta_3N_5 composite, similar to blank Ta_3N_5, its UV-vis absorption spectrum have a strong absorption band in range from 200 to 625 nm with a maximum at 415 nm and moderate intensity absorption band in range from 625 to 900 nm peaking at 750 nm (Figure 4b, color line). As mentioned above, the LSPR is strongly affected by many parameters such as morphology, size, and composition of the nanoparticles as well as the dielectric properties of the surrounding medium. The dielectric constant of Ta_3N_5 is estimated to be 110, which is much higher than those of Ta_2O_5 (~ 30) and H_2O (~ 1). When Au nanoparticles were embedded in Ta_3N_5 host lattice, the strong coupling between Au nanoparticles and Ta_3N_5 host lattice, and high dielectric constant of the Ta_3N_5 host lattice will lead to the big red shift of LSPR absorption band of Au nanoparticles and the increases of absorption intensity of Ta_3N_5 in UV/visible region. For example, the maximum LSPR bands absorption band shift from 518 nm to 750 nm, and the absorption intensity of the Nano Au/Ta_3N_5 composite in UV/visible absorption range from 200 to 625 nm is around 1.45 times higher than that of the blank Ta_3N_5 sample. Obviously, the embedding Au nanoparticles in Ta_3N_5 is responsible for the increased and new absorption bands in visible light region in Nano Au/Ta_3N_5 composite, which will contribute to its novel photocatalytic activities accordingly.

We have also investigated the absorption intensities of Nano Au/Ta_2O_5 composites as a function of annealing temperature. The UV-vis absorption spectra of Nano Au/Ta_2O_5 composites (Nano Au 1.08 mol% of Ta_2O_5) calcinated at different temperature are shown in Supporting Information 3 (SP3). It can be seen from SP3 that all UV-vis absorption spectra of Nano Au/Ta_2O_5 composites spectra show strong characterized LSPR absorption bands of Au nanoparticles ranging from 310 to 900 nm. The UV-vis absorption spectra have similar shape and show both bandgap absorption of Ta_2O_5 and the characterized SPR absorption of Au nanoparticles. The samples annealed at 550 ^oC also show characterized SPR absorption band of Au nanoparticles with comparable absorption intensity, although it is still in amorphous phase (shown in SP1) at current annealing temperature. The absorbance intensity does not change so much when calcination temperature is below 700 ^oC, however when calcination temperature is over 700 ^oC, the absorbance intensity decrease monotonely. Usually, the crystallinity of sample increases with increasing calcination temperature, which will lead to less defects and higher absorption intensity of the calcinated sample. On the other hand, higher calcinations temperature also will lead to serious aggregation of solid samples, which may lead to optical properties decrease accordingly, such as absorbance, fluorescence, etc..[18,19,50] It is also seen from SP3 that increasing calcination temperature caused a small red shift in the SPR absorption band, which might be ascribed to the aggregation and size growing up of Au nanoparticles in Nano Au/Ta_2O_5 composites when calcinating at higher temperature.

3.3 Photocatalytic performance of Nano Au/Ta_2O_5 composites

After Pt nanoparticles were loaded as cocatalyst on Nano Au/Ta_2O_5 composites, the composites' photocatalytic activities were measured for H_2 evolution from an aqueous methanol solution under visible light irradiation. Figure 5 shows the time course for the evolved H_2 of

Nano Au/Ta_2O_5 composite (Au 0 ~ 1.44 mol% of Ta_2O_5) sample calcinated at 700 ^oC. It is clearly seen from Figure 5 that there is no H_2 evolution for blank Ta_2O_5 (without Au nanoparticles embedding in Ta_2O_5, black dots) under the irradiation of visible light. However, for Nano Au/Ta_2O_5 composite, under the irradiation of visible light, it shows a new recreating photocatalytic activity of H_2 evolution from water comparing to blank Ta_2O_5. Obviously, in Nano Au/Ta_2O_5 composite catalysis the embedding Au nanoparticle is a very important parameter that determines the new recreating photocatalytic activity of the composites material.[30,54] When changing the amount of the embedding Au nanoparticles, several parameters, such as morphology, the intensity of absorption, light scattering, SPR and inner electromagnetic field varied simultaneously. The balanced combination of all these factors determines that generally an optimal Au nanoparticles embedding is observed for having the maximum photocatalytic activity. In the present case we prepared a series of Nano Au/Ta_2O_5 composites with different embedding concentration of Au nanoparticles by Sol-gel method and compared their photocatalytic activities for hydrogen generation from water in response to visible light with that of blank Ta_2O_5 devoid of Au nanoparticle embedding. The photocatalytic activities for H_2 evolution from water of five representative Nano Au/Ta_2O_5 composite samples and blank Ta_2O_5 are shown in Figure 5. As it can be seen from Figure 5 that the photocatalytic H_2 evolution rate of the Nano Au/Ta_2O_5 composite increases with increasing embedding Au nanoparticle content when Au nanoparticle content is lower than 1.08 mol % of Ta_2O_5, and then it reaches a remarkable maximum value of 55 μmol g^{-1} h^{-1}.[30] However, further increasing the content of embedding Au nanoparticles leads to a reduction of photocatalytic activity. This reduction is probably due to the increase of light scattering of samples with higher Au contents, which actually reduce the effective irradiation absorption in the reaction suspension solution.[55,56]

Furthermore, excessive Au nanoparticles embedded in Ta_2O_5 may in turn work as recombination centers and thus hinder the photocatalytic hydrogen production reaction.[55,57] Typically, the most active materials in Nano Au/Ta_2O_5 composites are those containing around 1.08 mol % Au nanoparticle embedding content.

As one of the noble metals, Pt nanoparticle has been widely used as a cocatalyst in photocatalytic water splitting over many different kinds of semiconductors.[58] Up to now, the highest photocatayltic activities for H_2 production from water response to visible-light irradiation are from photocatalysts loaded with Pt nanoparticles as cocatalyst.[58] In the case of the Pt-loaded Nano Au /Ta_2O_5 plasmonic photocatalyst, it is necessary to obtain a highest photocatalytic activity for hydrogen evolution from water with optimize amount of Pt nanoparticles loading as cocatalyst that facilitates the migration of electrons photogenerated from the conduction band of photocatalyst to the Pt cocatalyst. Here, the effect of the amount of Pt cocatalyst on the photocatalytic activities of Nano Au /Ta_2O_5 composite was investigated to determine the optimum amount of Pt loading. Supporting Information 4 (SP4) shows the dependence of the photocatalytic activity for H_2 evolution over Pt/Nano Au/Ta_2O_5 composite (Nano Au 1.08 mol% of Ta_2O_5) calcinated at 700 ^oC upon the amount of loading Pt nanoparticles. The photocatalytic activity of Nano Au/Ta_2O_5 composite is drastically increased upon increasing the loading amount of Pt nanoparticles and shows a maximum at 1.0 wt% for the loading amount of Pt nanoparticles. Thus the optimum loading amount of Pt is 1.0 wt% of Nano Au/Ta_2O_5 composite.

The photocatalytic activities of Nano Au/Ta_2O_5 composites change with theirs calcination temperatures. The H_2 evolution rate dependences on the calcination temperature of Nano Au/Ta_2O_5 composite are shown in Supporting Information 5 (SP5). It can be seen from SP5 that the H_2 evolution rate firstly increases monotonely before 700 ^oC, after that the H_2 evolution rate

decreases with increasing calcination temperature. Although, the absorption intensity of Nano Au/Ta_2O_5 composite does not change so much when calcination temperature is below 700 ^oC (shown in SP3), the crystallinity of Ta_2O_5 increase with increasing the calcinations. Usually, the higher crystallinity leads to the higher photocatalytic activity of Nano Au/Ta_2O_5 composite, and that the higher calcinations temperatures will increase the interfacial contact between Au nanoparticles and Ta_2O_5 host lattice, which will facilitate the charge carriers' communication between Au nanoparticles and Ta_2O_5 host lattice. However, when Nano Au/Ta_2O_5 composite's calcination temperature is over 700 ^oC, due to their decreased absorbance in visible light range (shown in SP2), its photocatalytic activity will decrease accordingly. Furthermore, the reduction in photocatalytic activity of Nano Au/Ta_2O_5 composite calcinated from 700 ^oC to 800 ^oC might be attributed to the decrease in their surface area caused by aggregation when calcinated at high temperature.

Usually, the electron donors/acceptors are used as sacrificial reagents in photocatalytic reactions to improve their photocatalytic efficiency for hydrogen/oxygen generation. When photocatalytic system is constructed in the presence of an electron donor, the photogenerated holes irreversibly oxidize the reducing electron donors instead of H_2O. Similarly, if the bottom of the conduction band of the photocatalyst is located at a more negative potential than the water reduction potential, this will facilitate water reduction by the photogenerated electrons in the conduction band. Furthermore, the sacrificial reagent can be used to detect the energy positions of conduction and valence band edges of photocatalyst.[30,54,55] Figure 6 shows the H_2 evolution amount of Nano Au/Ta_2O_5 composite dependence on different sacrificial reagents. Here, the inorganic sacrificial reagents, such as S^{2-}/SO_3^{2-}, and $Fe^{2+}(/Fe^{3+})$, and organic sacrificial reagents, such as CH_3OH, C_2H_5OH, C_3H_7OH, CH_3CHO and $(COOH)_2$ are used for H_2 generation in Nano

Au /Ta_2O_5 composite photocatalytic system. As shown in Figure 6, the photocatalytic activities of Nano Au /Ta_2O_5 composite decrease in the following sacrificial reagents sequence, $CH_3CHO > S^2/SO_3^{2-} \approx C_2H_5OH \approx CH_3OH > C_3H_7OH > (COOH)_2 > Fe^{2+}/(Fe^{3+})$ (almost zero). As it is known that the photocatalytic activities have close relationship with the standard oxidation reduction potential of sacrificial reagent, which show their capability of supplying/accepting electrons. The up sequences of sacrificial reagent contribution to photocatalytic activities basically agree with their standard oxidation reduction potential order.[54,55] The standard oxidation reduction potential of Fe^{2+}/Fe^{3+} is 0.77 eV, there is no photocatalytic activities when $Fe^{2+}/(Fe^{3+})$ is used as a sacrificial reagent for H_2 evolution in Nano Au /Ta_2O_5 photocatalytic system, which might be due to the oxidation reduction potential of the positively charged Au nanoparticles is lower than that of $Fe^{2+}/(Fe^{3+})$, and so the positively charged Au nanoparticles can not oxidize Fe^{2+} to Fe^{3+}.[30,58] The normal redox potential of O_2/H_2O is determinated to be 1.23 eV, which is higher than that of Fe^{2+}/Fe^{3+} (0.77 eV). Thus it can be deduced that the photoexcited Nano Au /Ta_2O_5 composite (the positively charged Au nanoparticles) can not oxidize water to get O_2, which was proved in the later experiment.

To further elucidate the role of the embedded Au nanoparticles in new recreating photoactivity of Nano Au/Ta_2O_5 composite response to visible light irradiation, we have measured the photocatalytic activity of blank Ta_2O_5 and Au nanoparticles solely for hydrogen evolution from water with the illumination of visible light under the same experimental conditions as those of Nano Au/Ta_2O_5 composites. The control experiments show as expected that the Ta_2O_5 and Au nanoparticles solely are devoid of any photocatalytic activity for hydrogen evolution from water under the excitation of visible light. Under the current situation, it is obviously that only Au nanoparticles combine with Ta_2O_5 host lattice will make Nano Au/Ta_2O_5

composite a new recreating photocatalytic activity for H_2 evolution from water in response to visible light irradiation.

We have also tested how morphology, structure and prepared methods influence the new recreating photocatalytic activity of Nano Au/Ta_2O_5 composite for H_2 evolution response to visible light irradiation. The same amount of Au nanoparticle (Au 1.08 mol % of Ta_2O_5) was loaded on Ta_2O_5 particle surface by impregnation. The sample was denoted as "surface configuration" comparing to the Nano Au embedding sample denoted as "embedded configuration". After Au nanoparticle loading on Ta_2O_5, the surface configuration sample was calcinated at 500 ^oC for 3 hours to make them close contact. For H_2 evolution, the prepared sample was processed as same procedures as those of embedded configuration sample done. The UV-vis absorption spectra of blank Ta_2O_5 (a), the embedded configuration Nano Au/Ta_2O_5 composite (b), and the surface configuration Nano Au/Ta_2O_5 composite (c) are shown in Figure 7a. The absorption spectrum of the stock solution of Au nanoparticles (d) is also shown in Figure 7a for comparison. From Figure 7a it can be seen that the UV-vis absorption spectra of the surface configuration Nano Au/Ta_2O_5 composite show comparable absorption intensity to that of the embedded configuration Nano Au/Ta_2O_5 composite, but obvious with wide absorption band and red shift of SPR of Au nanoparticle, which might be due to the Au nanoparticle size growing up during the later calcinations process. Figure 7b shows the time course for evolved H_2 of the surface configuration Nano Au/Ta_2O_5 composite (black dots and line) and the embedded configuration Nano Au/Ta_2O_5 composite (red dots and line) under the visible light excitation. From Figure 7b it can be seen clearly that under the same experiment conditions, although both embedded configuration and surface configuration Ta_2O_5/Au composites are active response to visible light excitation, but the photocatalytic activity of the embedded configuration Nano

Au/Ta_2O_5 composite is four times higher than that of the surface configuration Nano Au/Ta_2O_5 composite.

The above experiment results show that the morphology and structure of Ta_2O_5/Au composite play an important role for its photocatalytic activity. Firstly, when Au nanoparticle is loaded on the surface of Ta_2O_5, the Au nanoparticle and Ta_2O_5 host lattice cannot be connected as tightly as that of the embedded configuration Nano Au/Ta_2O_5 composite prepared by Sol-gel method. The interface contact resistance between Au nanoparticle and Ta_2O_5 in surface configuration Nano Au/Ta_2O_5 composite is higher than that in embedded configuration Nano Au/Ta_2O_5 composite, which will make the excited electrons transfer from Au nanoparticle to Ta_2O_5 become a little more difficult and leading to its lower photocatalytic activity accordingly. Secondly, the Au nanoparticles on Ta_2O_5 surface will shield and scatter the visible light, which will lead to its lower visible light absorbance (as shown in Figure 7a) and low photocatalytic activity. Finally, when the Au nanoparticle is loaded on the surface of Ta_2O_5, the high coverage of the Au nanoparticle may reduce the surface area of Ta_2O_5 in direct contact with the H_2O and thereby hinder the hydrogen evolution performance.[17,18,19,30]

In order to compare how Au nanoparticles influence the photocatalytic activities of Ta_2O_5 under the UV irradiation, we have also measured the photocatalytic activities of Ta_2O_5 and Nano Au/Ta_2O_5 composite for H_2 and O_2 evolution under the irradiation of UV light (a 300 W Xe lamp with a cold mirror of CM-2 in the wavelength range of 200 ~ 400 nm) under the same experiment conditions as those of visible light irradiation for H_2 and O_2 evolution except for excitation lights source. Figure 8a shows the H_2 evolution of Ta_2O_5 and Nano Au/Ta_2O_5 composite under the irradiation of UV. For H_2 evolution, as shown in Figure 8a, the photocatalytic activities of Nano Au/Ta_2O_5 composite are a little bit higher than that of blank

Ta_2O_5. For blank Ta_2O_5, it only can be excited by UV light from 200 to 310 nm due to its wide band gap limitation (shown in Figure 4a). But for Nano Au/ Ta_2O_5 composite, it absorbs UV light in range from 200 to 400 nm. Obviously, the embedding Au nanoparticles extend the absorption UV range from 310 to 400 nm due to SPR of Au nanoparticles embedded in Ta_2O_5 (shown in Figure 4a). It is supposed that the extended absorption range (310 ~ 400 nm) of UV light can also be used for H_2 evolution. So it is not surprise that the photocatalytic activities for H_2 evolution of Nano Au/ Ta_2O_5 composite are a little bit higher than that of blank Ta_2O_5 responding to UV light irradiation. At least, it can be concluded that the Au nanoparticles embedded in Ta_2O_5 will not kill the H_2 photocatalytic activities of Ta_2O_5 under the irradiation of UV light. However, for O_2 evolution, as shown in Figure 8b, the situation is completely different. Under the irradiation of UV light, the blank Ta_2O_5 shows high photocatalytic activities for O_2 evolution. But for Nano Au/ Ta_2O_5 composite, there is no O_2 evolution when it is irradiated by UV light. Obviously, the photocatalytic activity for O_2 evolution was killed by embedded Au nanoparticles in Ta_2O_5 even it is excitated by UV light. When Au nanoparticles were embedded in Ta_2O_5 host lattice, they would introduce a few new energy levels. Due to the mismatch of these new energy levels to the valance band of the Ta_2O_5, the photocatalytic activities for O_2 evolution was quenched. In the front section, we have shown the photocatalytic activities of Nano Au/ Ta_2O_5 composite for H_2 evolution from water was quenched by sacrificial reagent of $Fe^{2+}/(Fe^{3+})$, which might be due to the redox potential of the positively charged Au nanoparticles is lower than that of Fe^{3+}/Fe^{2+}. The standard electrode potential of Fe^{3+}/Fe^{2+} is determined to be 0.77 eV, so it can be deduced that the redox potential of the positively charged Au nanoparticles is lower than that of O_2/H_2O (1.23 eV). Under the excited of UV light, the photon-generated carrier (holes) will be transferred from the valence band of Ta_2O_5 to the positively charged Au nanoparticles, which will lead to the

quench of O_2 evolution accordingly in Nano Au/ Ta_2O_5 composite photocatalytic system illuminated by UV light. The possible mechanism is shown in Figure 9.

As discussed in introduction section, noble metal nanoparticle SPR improves the solar-energy-conversion efficiency on nearby semiconductors by charge transfer mechanism, near-field electromagnetic effect mechanism and photon scattering effect mechanism.[17,18] For both near-field electromagnetic effect and photon scattering effect, the enhancement of photoactivity could be observed only when the SPR of Au nanoparticle spectrally overlaps with the absorption of semiconductor.[17,18] In Nano Au/Ta_2O_5 composite system, as shown in Figure 4a, there is no absorption spectra overlap between the SPR of Au nanoparticles and Ta_2O_5 in visible region, which eliminate the new recreating photoactivity due purely to the near-field electromagnetic effect and the resonant photon scattering effect. A possible mechanism for plasmon-induced new recreating photocatalytic activity of Nano Au/Ta_2O_5 composite for hydrogen evolution from water response to visible-light might be the plasmon-assisted direct electron transfer (DET) reaction from Au nanoparticle to the conduction band of Ta_2O_5.[59] In Nano Au/Ta_2O_5 composite, it is believed that Au nanoparticle serve as a photosensitizer that absorbs resonant photons, generates high-energy (or excited) electrons upon SPR excitation and injects them into the conduction band of the adjacent Ta_2O_5 semiconductor. With the efficient supply of high-energy (or excited) electrons upon SPR excitation, The Ta_2O_5 semiconductors decorated with Au nanoparticle will show a significantly new recreating photoactivity for hydrogen evolution from water under visible-light illumination.[26,27]

It has been reported that DET occurs from the plasmonic metal to the conduction band of the semiconductor when they are in direct contact.[17] DET depends on the alignments of the band levels of the semiconductor and Fermi level of the plasmonic metal, so it is possible for electrons

or holes to be transferred from the metal into the semiconductor at energies below the band gap if the electronic energy levels match.[25,60] To better understand the mechanism of plasmon-enhanced photoactivity in the current system, a schematic illustrating the energic electrons transfer from Au nanoparticle to Ta_2O_5, photocatalytic mechanism of Ta_2O_5 with/without Au nanoparticles embedding for hydrogen and oxygen evolution respectively are shown in Figure 9. In Nano Au/Ta_2O_5 composite, illuminating Au nanoparticle with visible light excites surface plasmons, these excited surface plasmons will decay rapidly, and produce many energetic electrons (often referred to as electron-hole pairs, even though both these species coexist in the metal's conduction band). The energetic electrons transiently occupy normally empty states in the gold's conduction band above the Fermi energy level. A significant fraction of these excited electrons are transferred to the conduction band of Ta_2O_5 for hydrogen evolution. This process leaves energetic positives charges (sometimes referred to figuratively as holes) on the gold nanoparticles. To maintain charge equilibrium, the positively charged Au nanoparticles receive e^- from the electron donor (the anode sacrificial regent, such as methanol, ethanol, and formic acid etc..).[56] Under the excitation of UV light, due to the energy levels match, the photo-generated holes are transferred from valence band of Ta_2O_5 to the positively charged Au nanoparticles (shown in Figure 9), so it will lead to the quench of O_2 evolution in Nano Au/Ta_2O_5 composite in response to visible and UV light irradiation.

3.4 Photocatalytic performance of Nano Au/Ta_3N_5 composites

When Au nanoparticles were embedded in Ta_3N_5 host lattice, the strong coupling effects of Au nanoparticles and the Ta_3N_5 host lattice lead to the enhancement of its photocatalytic activities for hydrogen evolution in response to visible light irradiation. Figure 10 shows the time course for evolved H_2 of the five representative Nano Au/Ta_3N_5 composite samples (Au

nanoparticle is 0.54 ~2.17 mol% of Ta_3N_5). The photocatalytic activities for hydrogen evolution in response to visible light irradiation of blank Ta_3N_5 are also shown here for comparison. From Figure 10, it can be seen clearly that the photocatalytic H_2 production rates of Nano Au/Ta_3N_5 composite increase with increasing Au nanoparticle content first, reaching a maximum value when Au nanoparticle is 1.08 mol % of Ta_3N_5, and then decrease with increasing its embedding concentration. It is also shown in Figure 10 that in the low embedding Au nanoparticle concentration (Au nanoparticle is 0.54 ~1.63 mol% of Ta_3N_5), the Nano Au/Ta_3N_5 composite's photocatalytic activities for hydrogen evolution in response to visible light irradiation is higher than that of blank Ta_3N_5. Further increase the embedding Nano Au concentration to 2.17 mol %, the Nano Au/Ta_3N_5 composite's photocatalytic activities for hydrogen evolution in response to visible light irradiation is lower than that of blank Ta_3N_5. Obviously, the increased/decreased photocatalytic activities of Nano Au/Ta_3N_5 composite for hydrogen evolution in response to visible light irradiation come from the SPR effect of the embedding Au nanoparticles. Moderated amount of embedding Au nanoparticles in Ta_3N_5 will improve its photocatalytic activity, excessive Au nanoparticles amount may in turn work as recombination centers and thus hinder the photocatalytic hydrogen production reaction accordingly.[55,57]

As discussed in front section, the enhanced photocatalytic activities of Nano Au/Ta_3N_5 composite might due to charge transfer, near-field electromagnetic effect and resonant photon scattering effect induced by SPR of Au nanoparticles. From Figure 4b it can be seen clearly that there is a big overlap within visible light range for the SPR spectrum of Au nanoparticles and the absorption spectrum of semiconductor Ta_3N_5, which favor of near-field electromagnetic effect and resonant photon scattering effect. Usually, the significant resonant photon scatting effect and enhancements to the optical path length are only seen in large plasmonic metal nanoparitcles (>

50 nm).[17] The Au nanoparticles embedded in Ta_3N_5 host lattice is around 15 ~ 20 nm in diameter, eliminating photocatalytic activities enhancements due purely to the resonant photon scattering effect. So the enhanced photocatalytic activities of Nano Au/Ta_3N_5 composite (comparing to blank Ta_3N_5) for hydrogen evolution in response to visible light irradiation might be ascribed to the near-field electromagnetic effect induced by SPR of Au nanoparticles.

The electromagnetic field of incident light couples with the oscillations of conduction electrons in gold particles, resulting in strong-field enhancement of the local electromagnetic fields near the surface of gold nanoparticles.[17,26,27] Such enhanced local field strength can be much higher than the applied electromagnetic field (i.e., incident light).[32] Thus, it is suggested that when the wavelength of incident light matches with the SPR band of Au nanoparticles, the resonance of the electrons was induced, as if forming an extra electron magnetic field to enhance the light effect, facilitate the selective formation of electron-hole pairs in the near-surface region of the neighboring Ta_3N_5 semiconductor. Furthermore, the enhanced local field at the interface of Au nanoparticle and Ta_3N_5 induced by SPR will facilitate the separation and migration of the photogenerated electrons and holes to their active sites for redox reactions. All these positive elements will finally result in the enhancement of photocatalytic activity of Nano Au/Ta_3N_5 composite for hydrogen evolution accordingly.

Comparing the absorbance of Ta_3N_5 and Nano Au/Ta_3N_5 composite (shown in Figure 4b), it also can be seen that the SPR of Au nanoparticles embedded in Ta_3N_5 has induced the enhancement absorbance of the Nano Au/Ta_3N_5 composite to 1.45 times higher than that of the blank Ta_3N_5 in the visible region (420 ~ 536 nm and 625 to 900 nm, shown in Figure 4b). Considering both the conduction bands of Ta_3N_5 and Ta_2O_5 are mainly consisted of Ta5d orbital, so the potentials of the bottoms of the conduction bands of Ta_3N_5 and Ta_2O_5 are almost the

same.[61] It is reasonable that the energetic (or excited) electrons (e^-) in Au nanoparticles induced by SPR effect might be transferred to conduction band of Ta_3N_5 for hydrogen evolution as has happened in Nano Au/Ta_2O_5 composite. Therefore, the DET effect induced by SPR might also contribute to the enhancement of photocatalytic activity of Nano Au/Ta_3N_5 composite to some extent. Based on the above analysis, the enhanced photocatalytic activities of Nano Au/Ta_3N_5 composite (comparing to blank Ta_3N_5) for hydrogen evolution in response to visible light irradiation might be ascribed to synergetic effect of the near-field electromagnetic effect and the charge transfer induced by SPR of embedded Au nanoparticles.

We have measured the photocatalytic activity of Nano Au/Ta_3N_5 composites for oxygen evolution from water response to visible light irradiation. Unfortunately, similar to Nano Au/Ta_2O_5 composite, the photocatalytic activity of Nano Au/Ta_3N_5 composite for oxygen evolution from water response to visible light irradiation was quenched by the embedded Au nanoparticles, which might be due to the mismatch of energy levels of the excited Au nanoparticles and Ta_3N_5 host lattice. Obviously, the Au nanoparticle embedded in Ta_2O_5/Ta_3N_5 has played double roles. On the one hand, it promotes an active photocatalytic activity for hydrogen evolution; on the other hand, it introduces a negative photocatalytic activity for oxygen evolution from water response to UV/visible light irradiation.

4 Conclusions

In summary, we have demonstrated a new recreating photocatalytic activity for hydrogen evolution of Nano Au/Ta_2O_5 composite and a significantly enhanced photocatalytic activity for hydrogen evolution of Nano Au/Ta_3N_5 composite response to visible light irradiation by embedding Au nanoparticle in Ta_2O_5 and Ta_3N_5 host lattices, respectively. The new recreating photocatalytic activity of Nano Au/Ta_2O_5 composite response to visible light excitation might be

due to the charge transfer from Au nanoparticle to Ta_2O_5 host lattice induced by SPR of Au nanoparticle upon visible light irradiation. The enhanced photocatalytic activity of Nano Au/Ta_3N_5 composite in visible region for hydrogen evolution comparing with blank Ta_3N_5 might come from the synergetic effect of charge transfer and near-field electromagnetic effect induced by SPR of embedded Au nanoparticles. The ability to tune and expand the photoactivity of semiconductors in UV and the visible light region through SPR effect makes it possible to design novel and efficient plasmon-photocatalyst for photochemical solar hydrogen evolution.

Acknowledgements

The authors would like to thank Prof. Kazunari Domen (The University of Tokyo, Japan) and Prof. Kazuhiro Takanabe (King Abdullah University of Science and Technology, Saudi Arabia) for their fruitful comments. This project is financially supported by the National Natural Science Foundation of China (NSFC 21161015, 21165013), the Natural Science Foundation of the Jiangxi Province of China (2009GZH0082), the Natural Science Foundation of the Jiangxi Higher Education Institutions of China (GJJ09180, GJJ14513), the open fund of Key Laboratory of Jiangxi Province for Persistant Pollutants Control and Resources Recycle, and Nanchang Hangkong University Doctoral Foundation.

Supporting Information available:

Supporting figures for the XRD patterns of Nano Au/Ta_2O_5 composite annealed at different temperature, the EDS of Nano Au/Ta_2O_5 (Ta_3N_5)-Pt, UV-Vis diffuse reflectance spectra of Nano Au/Ta_2O_5 composite annealed at different temperature, the dependence of the photocatalytic

activity of Au/Ta_2O_5 composite on the loading amount of Pt, and typical time course for H_2 evolution from Nano Au/Ta_2O_5 composite annealed at different temperature. This material is available free of charge via the Internet.

References

1 M. A. Prog. Green, *Photovoltaics*, 2009, **17**, 183.

2 N. Q. Wu, J. Wang, D. Tafen, H. Wang, J. G. Zheng, J. P. Lewis, X. Liu, S. S. Leonard, A. Manivannan, *J. Am. Chem. Soc.*, 2010, **132**, 6679.

3 K. Iwashina, A. Kudo, *J. Am. Chem. Soc.*, 2011, **133**, 13272.

4 K. Maeda, K. Domen, *J. Phys. Chem. Lett.*, 2010, **1**, 2655.

5 Y. Hou, A. B. Laursen, J. Zhang, G. Zhang, Y. Zhu, X. Wang, S. Dahl, I. Chorkendorff, *Angew. Chem., Int. Ed.*, 2013, **52**, 3621.

6 S. Li, L. Zhang, T. Jiang, L. Chen, Y. Lin, D. Wang, T. Xie, *Chemistry - A European Journal*, 2014, **20**, 1.

7 G. Zhang, M. Zhang, X. Ye, X. Qiu, S. Lin, X. Wang, *Adv. Mater.*, 2014, **26**, 4.

8 Y. Qu, W. Zhou, L. Jiang, H. Fu, *RSC Advances*, 2013, **3**, 18305.

9 J. Xie, H. Zhang, S. Li, R. Wang, X. Sun, M. Zhou, J. Zhou, X. W. Lou, Y. Xie, *Adv. Mater.*, 2013, **25**, 40.

10 R. Dong, B. Tian, C. Zeng, T. Li, T. Wang, J. Zhang, *J. Phys. Chem. C*, 2013, **117**, 213.

11 K. Maeda, T. Takata, M. Hara, N. Saito, Y. Inoue, H. Kobayashi, K. Domen, *J. Am. Chem. Soc.*, 2005, **127**, 8286.

12 Z. G. Zou, J. H. Ye, K. Sayama, H. Arakawa, *Nature*, 2001, **414**, 625.

13 X. Chen, S. Shen, L. Guo, S. S. Mao, *Chem. Rev.*, 2010, **110**, 6503.

14 K. Maeda, K. Teramura, D. Lu, T. Takata, Nobuo. Saito, Y. Inoue, and K. Domen, *Nature*, 2006, **440**, 295.

15 K. Maeda, K. Teramura, T. Takata, M. Hara, N. Saito, K. Toda, Y. Inoue, H. Kobayashi, K. Domen, *J. Phys. Chem. B*, 2005, **109**, 20504.

16 J. Kou, Z. Li, Y. Guo, J. Gao, M. Yang, Z. J. Mol. Zou, *Catal. A: Chem.*, 2010, **325**, 48.

17 S. K. Cushing, J. Li, F. Meng, T. R. Senty, S. Suri, M. Zhi, M. Li, A. D. Bristow, N. J. Wu, *Am. Chem. Soc.*, 2012, **134**, 15033.

18 P. A. Desario, J. J. Pietron, T. H. Brintlinger, L. C. Szymczak, D. R. Rolison, *J. Phys. Chem. C*, 2013, **117**, 15035.

19 Y. C. Pu, G. Wang, K. D. Chang, Y. Ling, Y. K. Lin, B. C. Fitzmorris, Ch. M. Liu, X. Lu, Y. Tong, J. Z. Zhang, Y. J. Hsu, Y. Li. *Nano Lett.*, 2013, **13**, 3817.

20 M. R. Jones, K. D. Osberg, R. J. Macfarlane, M. R. Langille, C. A. Mirkin, *Chem. Rev.*, 2011, **111**, 3736.

21 M. Brown, T. Suteewong, R. S. Kumar, V. D'Innocenzo, A. Petrozza, M. M. Lee, U. Wiesner, H. J. Snaith, *Nano Lett.*, 2011, **11**, 438.

22 S. D. Standridge, G. C. Schatz, J. T. Hupp, *J. Am. Chem. Soc.*, 2009, **131**, 8407.

23 Y. Ide, M. Matsuoka, M. Ogawa, *J. Am. Chem. Soc.*, 2010, **132**, 16762.

24 Q. Zhang, D. Q. Lima, I. Lee, F. Zaera, M. Chi, Y. Li, *Angew. Chem., Int. Ed.*, 2011, **123**, 7226.

25 C. Hu, T. Peng, X. Hu, Y. Nie, X. Zhou, J. Qu, H. He, *J. Am. Chem. Soc.*, 2010, **132**, 857.

26 I. Thomann, B. A. Pinaud, Z. Chen, B. M. Clemens, T. F. Jaramillo, M. L. Brongersma, *Nano Lett.*, 2011, **11**, 3440.

27 Z. Liu, W. Hou, P. Pavaskar, M. Aykol, S. B. Cronin, *Nano Lett.*, 2011, **11**, 1111.

28 Y. Tian, *T.* Tatsuma, *J. Am. Chem. Soc.*, 2005, **127**, 7632.

29 G. Wang, H. Wang, Y. Ling, Y. Tang, X. Yang, R. Fitzmorris, C. Wang, J. Zhang, Y. Li, *Nano Lett.*, 2011, **11**, 3026.

30 C. G. Silva, R. Juárez, T. Marino, R. Molinari, and H. García, *J. Am. Chem. Soc.*, 2011, **133**,

595.

31 A. Furube, L. Du, K. Hara, R. Katoh, M. Tachiya, *J. Am. Chem. Soc.*, 2007, **129**, 14852.

32 J. Chen, J. C. S. Wu, P. C. Wu, D. P. Tsai, *J. Phys. Chem. C*, 2011, **115**, 210.

33 H. Wang, T. You, W. Shi, J. Li, L. Guo, *J. Phys. Chem. C*, 2012, **116**, 6490.

34 D. B. Ingram, S. Linic, *J. Am. Chem. Soc.*, 2011, **133**, 5202.

35 H. Choi, W. Chen, P. Kamat, *ACS Nano*, 2012, **6**, 4418-4427.

36 Y. Shiraishi, D. Tsukamoto, Y. Sugano, A. Shiro, S. Ichikawa, S. Tanaka, T. Hirai, *ACS Catal.*, 2012, **2**, 1984-1992.

37 Y. Noda, B. Lee, K. Domen, J. N. Kondo, *Chem. Mater.*, 2008, **20**, 5361.

38 Y. Takahara, J. N. Kondo, T. Takata, D. Lu, K. Domen, *Chem. Mater.*, 2001, **13**, 1194.

39 M. Uchida, J. N. Kondo, D. Lu, K. Domen, *Chem. Lett.*, 2002, 498.

40 A. Lezau, B. Skadtchenko, M. Trudeau, D. M. Antonelli, *J. Chem. Soc., Dalton Trans.*, 2003, 4115.

41 C. Yue, L. Qiu, M. Trudeau, D. Antonelli, *Inorg. Chem.*, 2007, **46**, 5084.

42 C. Yue, M. Trudeau, D. Antonelli, *Chem. Commun.*, 2006, 1918.

43 W. Chen, A. Ishikawa, H. Fujisawa, T. Takata, J.N. Kondo, M. Hara, M. Kawai, Y. Matsumoto, K. Domen, *J. Phys. Chem. B*, 2003, **107**, 1798.

44 M. Hara, G. Hitoki, T. Takata, J.N. Kondo, H. Kobayashi, K. Domen, *Catal. Today*, 2003, **78**, 555.

45 G. Hitoki, A. Ishikawa, T. Takata, J.N. Kondo, M. Hara, K. Domen, *Chem. Lett.*, 2002, 736.

46 Y. Li, T. Takata, D. Cha, K. Takanabe, T. Minegishi, J. Kubota, K. Domen, *Adv. Mater.*, 2013, **25**, 125.

47 H. Tong, S. Ouyang, Y. Bi, N. Umezawa, M. Oshikiri, J. Ye. *Adv. Mater.*, 2012, **24**, 229.

48 X. Liu, L. Zhao, K. Domen, K. Takanabe, *MRS Bull.*, 2014, **49**, 58.

49 C. Ziegler, A. Eychmüller, *J. Phys. Chem. C*, 2011, **115**, 4502.

50 X. Liu, J. Lin, *J. Mater. Chem.*, 2008, **18**, 221.

51 A.F. Wells, (1947). *Structural Inorganic Chemistry*. Oxford: Clarendon Press.

52 R. Nashed, W. Hassan, Y. Ismail, N. Allam, *Phys. Chem. Chem. Phys.*, 2013, **15**, 1352.

53 IOP Conf. Series: *Materials Science and Engineering*, 2012, **34**, 012009.

54 S. Naya, T. Nikawa, K. Kimura, H. Tada, *ACS Catalysis*, 2013, **3**, 903.

55 J. Zhang, Y. Wang, J. Zhang, Z. Lin, F. Huang, J. Yu, *ACS Appl. Mater. Interfaces*, 2013, **5**, 1031.

56 D. Tsukamoto, Y. Shiraishi, Y. Sugano, S. Ichikawa, S. Tanaka, T. Hirai, *J. Am. Chem. Soc.*, 2012, **134**, 6309.

57 A. Kubacka, M. Fernández-García, Gerardo. Colón, *Chem. Rev.*, 2012, **112**, 1555.

58 X. Chen, S. Shen, L. Guo, S. S. Mao, *Chem. Rev.*, 2010, **110**, 6503.

59 X. Shi, K. Ueno, N. Takabayashi, H. Misawa, *J. Phys. Chem. C*, 2013, **117**, 2494.

60 P. Christopher, D. B. Ingram, S. Linic, *J. Phys. Chem. C*, 2010, **114**, 9173.

61 K. Maeda, K. Domen, *J. Phys. Chem. C*, 2007, **111**, 7851.

Captions for the Figures

Figure 1 XRD patterns of Ta_2O_5 NCs (a), Nano Au/Ta_2O_5 composite (b, Nano Au 1.44 mol% of Ta_2O_5) annealed at 750 ^oC and Ta_3N_5 NCs (c), Nano Au/ Ta_3N_5 composite (d, Nano Au 2.17 mol% of Ta_3N_5) nitrided at 750 ^oC.

Figure 2 The FE-SEM micrographs of Ta_2O_5 NCs (a), Nano Au/Ta_2O_5 composite (b) annealed at 750 ^oC and Ta_3N_5 NCs (c), Nano Au/ Ta_3N_5 composite (d) nitrided at 750 ^oC.

Figure 3 The TEM of Au nanoparticle (a), high-angle annular dark-field STEM images of blank Ta_2O_5 (b), Nano Au/Ta_2O_5 (c), EDS of Nano Au/Ta_2O_5 (d), high-angle annular dark-field STEM images of blank Ta_3N_5 (e), Nano Au/Ta_3N_5 (f), EDS of Nano Au/ Ta_3N_5 (g) and HRTEM of Nano Au/Ta_3N_5 loaded with Pt nanoparticle as cocatalyst (h).

Figure 4 The UV-Vis diffuse reflectance spectra of Nano Au/Ta_2O_5 composites (a, Nano Au 0 ~ 1.44 mol.% of Ta_2O_5) annealed at 750 ^oC and Nano Au/ Ta_3N_5 composites (b, Nano Au 0 ~ 2.17 mol.% of Ta_3N_5) nitrided at 750 ^oC. The absorption spectrum of the Au nanoparticles stock solution is shown in Figure 4 for comparison.

Figure 5 Typical time course for H_2 evolution from Nano Au/Ta_2O_5 composite (Au nanoparticle 0 ~ 1.44 mol% of Ta_2O_5). Reaction conditions: Catalyst, 0.06g (1 wt.% Pt cocatalyst); 10 vol.% methanol solution (100 ml); light source: a 300-W Xe lamp equipped with a cold mirror (CM-1) and a cutoff filter ($\lambda > 420$ nm). The vertical line shows the error bar.

Figure 6 Dependence of the photocatalytic activity of Au/Ta_2O_5 composite for H_2 evolution on different sacrificial regents. The vertical line shows the error bar.

Figure 7 The UV-Vis diffuse reflectance spectra of Ta_2O_5, embedded configuration Nano Au/Ta_2O_5 composite, surface configuration Nano Au/Ta_2O_5 composite, the absorption spectrum of the Au nanoparticles stock solution (a); and typical time course for H_2

evolution from Nano Au/Ta_2O_5 composite (b, red dots and line for embedded configuration and black dots and line for surface configuration). The vertical line shows the error bar.

Figure 8 Typical time course for H_2 (a) and O_2 (b) evolution from blank Ta_2O_5 and Nano Au/Ta_2O_5 composite (Au nanoparticle 1.08 mol.% of Ta_2O_5). Reaction conditions: Catalyst, 0.06g (1 wt.% Pt cocatalyst); 10 vol.% methanol solution (100 ml) for H_2 evolution; 100 ml H_2O, 0.01 M $AgNO_3$, 0.10 g La_2O_3 for O_2 evolution; light source: a 300-W Xe lamp equipped with a cold mirror (CM-2). The vertical line shows the error bar.

Figure 9 Proposed mechanism of hydrogen evolution for blank Ta_2O_5 and Nano Au/Ta_2O_5 composite.

Figure 10 Typical time course for H_2 evolution from Nano Au/Ta_3N_5 composite (Au nanoparticle 0 ~ 2.17 mol% of Ta_3N_5). Reaction conditions: Catalyst, 0.06g (1 wt.% Pt cocatalyst); 10 vol.% methanol solution (100 ml); light source: a 300-W Xe lamp equipped with a cold mirror (CM-1) and a cutoff filter ($\lambda > 420$ nm). The vertical line shows the error bar.

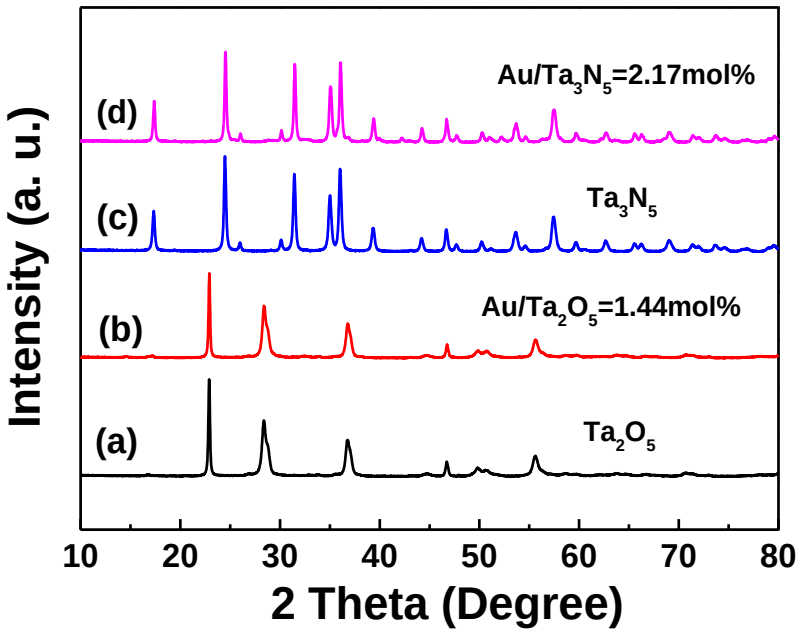

Figure 1

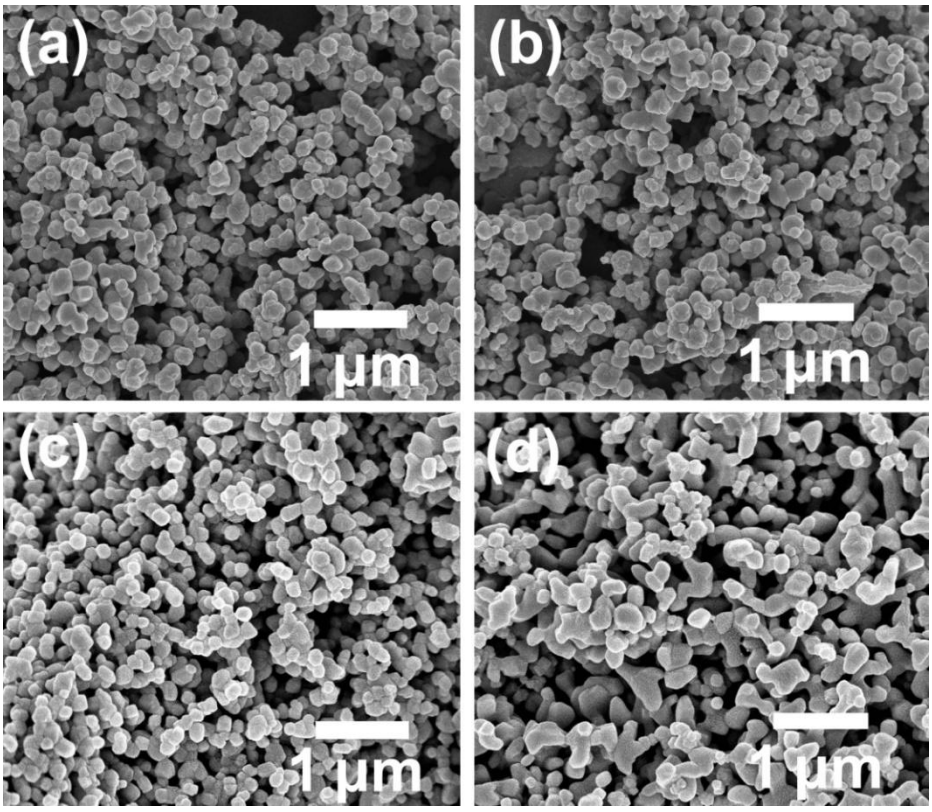

Figure 2

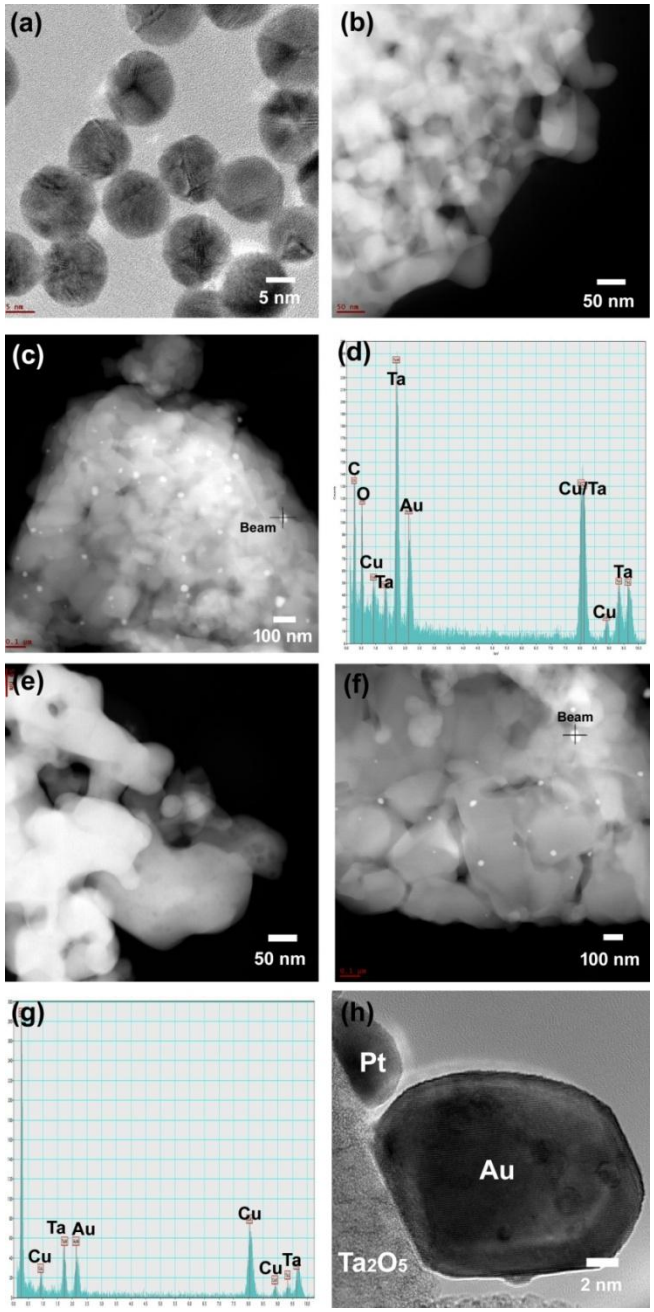

Figure 3

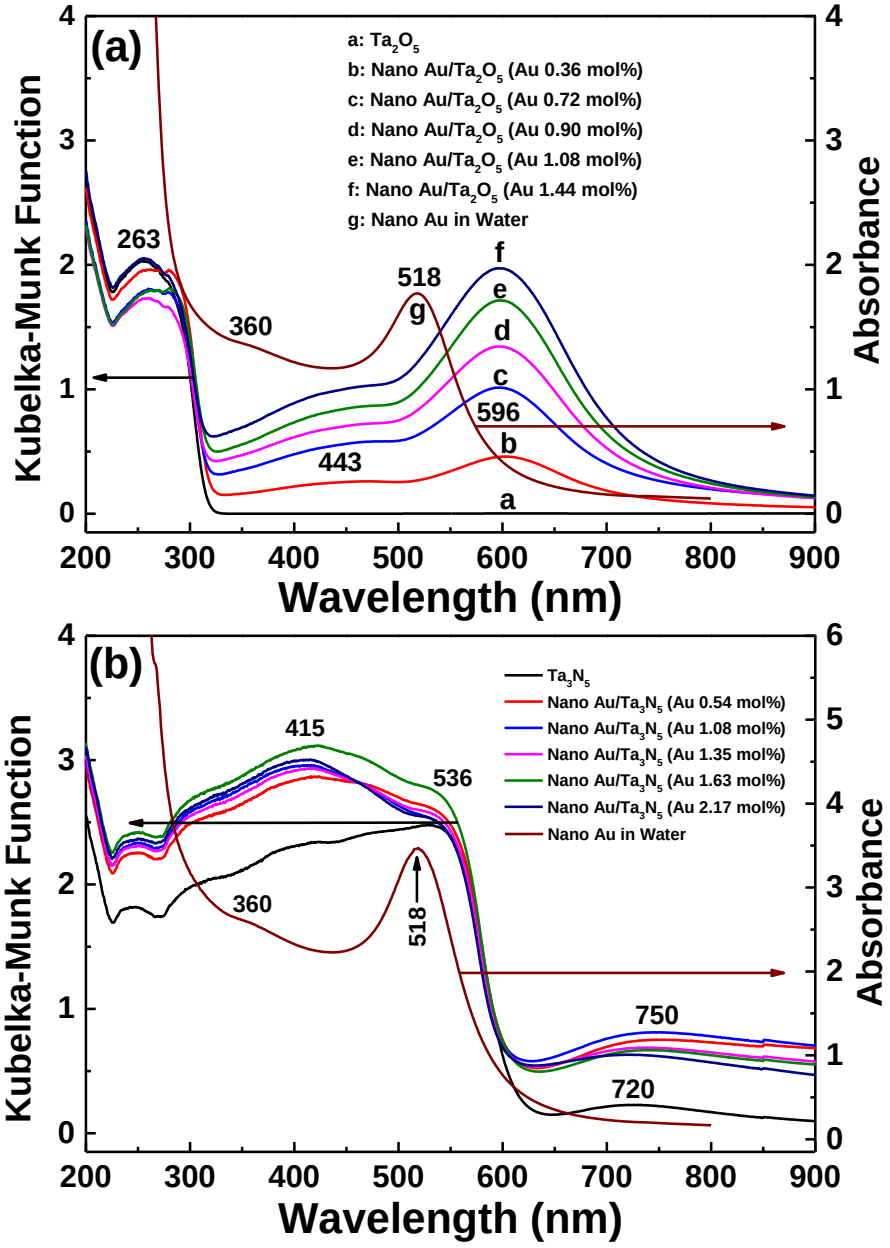

Figure 4

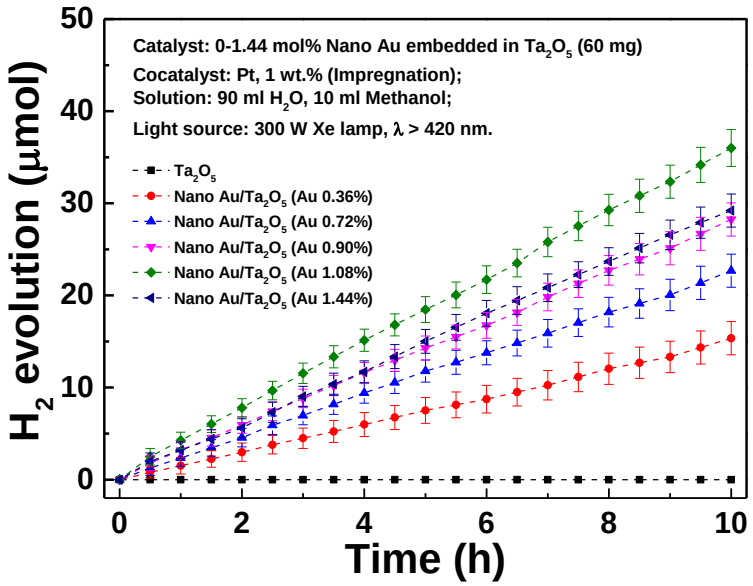

Figure 5

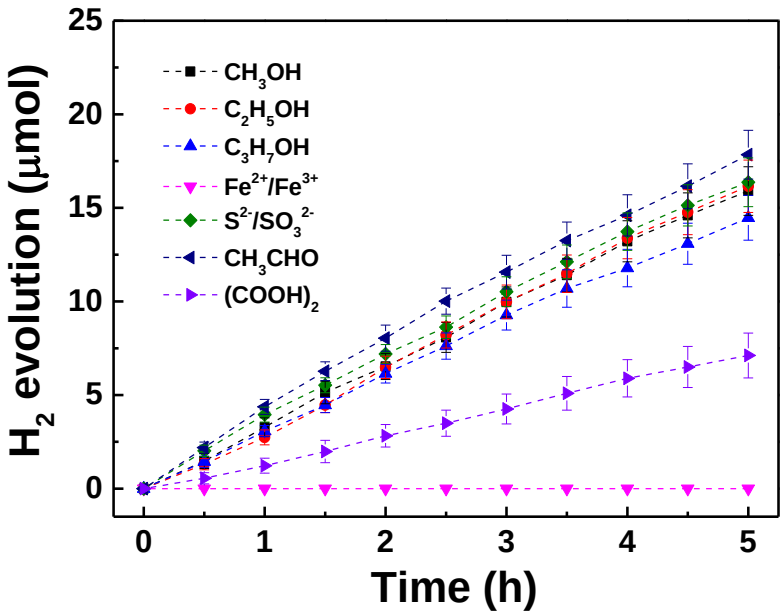

Figure 6

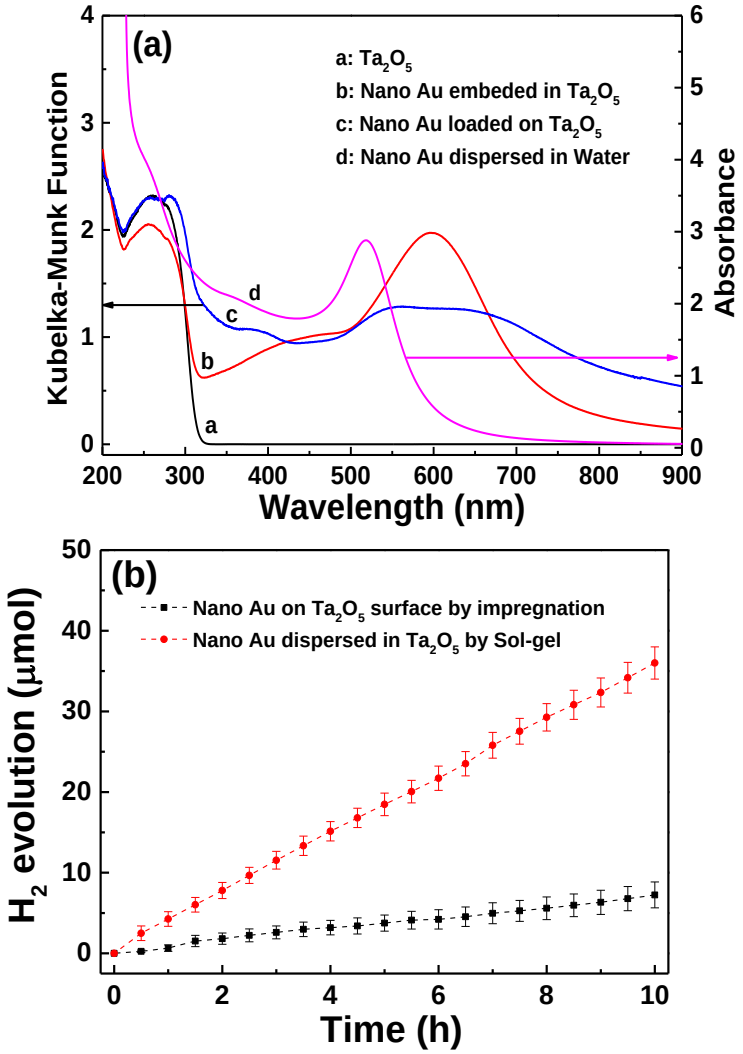

Figure 7

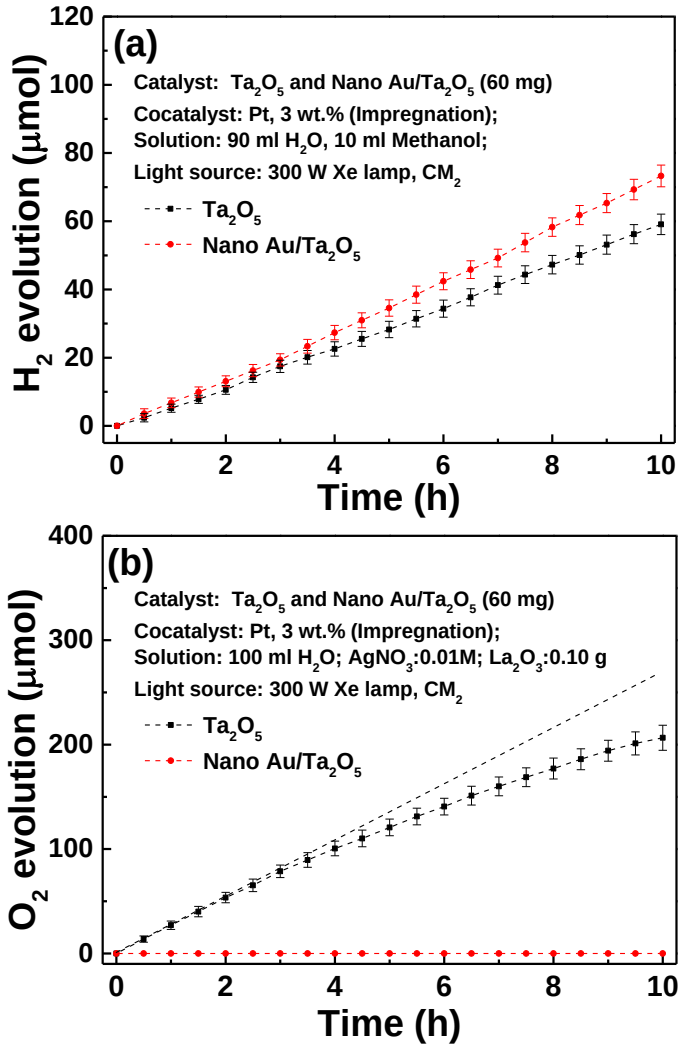

Figure 8

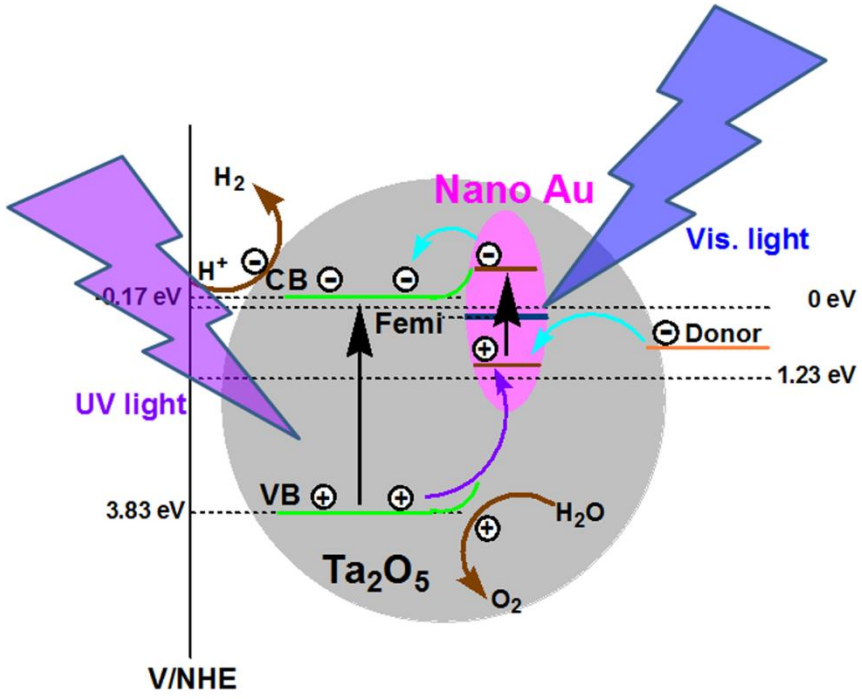

Figure 9

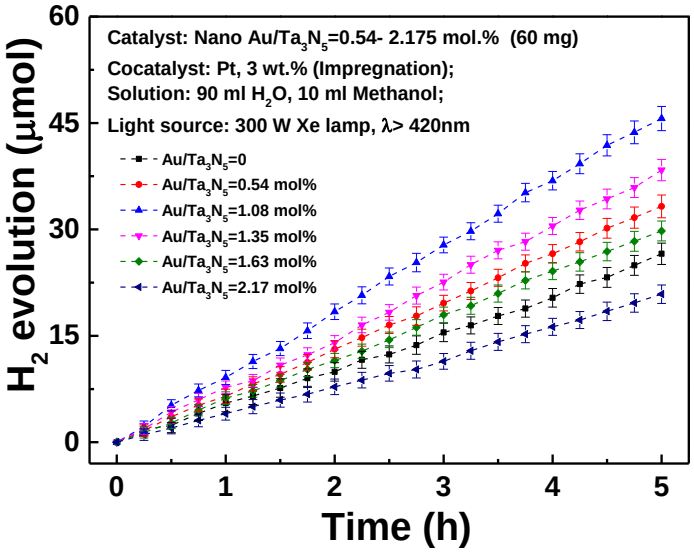

Figure 10